Broadband Ultra-Sensitive Adiabatic Magnetometer

Savukov, Igor Mykhaylovych
Kim, Young Jin

To be published in:

DOI to publisher's version: 10.1109/SAS51076.2021.9530142

Broadband Ultra-sensitive Adiabatic Magnetometer

Igor Savukov and Young Jin Kim
MPA-Quantum, Los Alamos National Laboratory, MS-D454, Los Alamos, New Mexico 87545, USA
(email: isavukov@lanl.gov)

***Abstract*—We introduce a new ultra-sensitive adiabatic magnetometer that has a broad bandwidth and can operate in the presence of magnetic fields and gradients. It follows conceptually typical implementations of atomic magnetometers based on alkali-metal vapor cells and lasers for optical pumping and optical Faraday effect detection, while its unique feature is a measurement of an oscillating magnetic field along the probe beam direction at frequencies lower than the resonant frequency, proportional to a static magnetic field along the pump beam direction. The bandwidth of the adiabatic magnetometer scales as the strength of the field along the pump beam. From our theoretical studies it is expected that the adiabatic magnetometer can reach 1 fT sensitivity with a bandwidth of 10 kHz, which any type of atomic magnetometers cannot achieve. Among anticipated various applications of this adiabatic magnetometer are biomagnetic sensing, nuclear magnetic resonance detection, and alkali-metal density measurements. We experimentally conducted alkali-metal density measurements, as an example of applications.**

***Index Terms*—Atomic magnetometer; adiabatic magnetometer; broad bandwidth; high field sensitivity; alkali-metal density**

I. Introduction

Various types of magnetometers based on atomic or nuclear spins, such as M_x and M_z magnetometers [1], nonlinear magneto-optical rotation (NMOR) magnetometers [2], helium magnetometers [3], rely on resonant operation. In case of the most sensitive spin-exchange relaxation-free (SERF) magnetometer based on alkali-metal vapor [4], [5], the resonance frequency is set to zero, while in the radio-frequency (RF) magnetometer the resonance frequency is set by a bias field [6].

Scalar magnetometers [7] are realized by measuring the change of the resonance frequency, when an oscillating magnetic field is applied with a frequency close to the resonance frequency of an RF magnetometer [6]. However, many of these magnetometers require tuning processes that take time. SERF magnetometers require zeroing magnetic fields, which sometimes is difficult, especially in an unshielded environment. Scalar magnetometers require finding the resonance frequency and might have difficulty operating in the presence of gradients. Another problem in the resonant operation is the limited bandwidth. SERF magnetometers have a several to 100 Hz bandwidth [4], while RF magnetometers about 100 Hz to 1 kHz [6], [9].

In this letter, we introduce a new type of atomic magnetometer whose operation is based on adiabatic following. In principle, in atomic magnetometers unpaired electron spins of alkali-metal vapor are manipulated with lasers for pumping and probing to sense magnetic fields. The new adiabatic magnetometer has multiple advantages over the resonance-based magnetometers, such as broadband operation, operation in the presence of magnetic fields and gradients, and easy tuning. Importantly, the adiabatic magnetometer can have high magnetic field sensitivity on the order of 1 fT/Hz$^{1/2}$ based on theoretical calculation. Because of its high sensitivity and broadband operation, we anticipate various applications of the magnetometer, e.g., in biomagnetic sensing.

II. Principles

A. Adiabatic Following

Theory of adiabatic following is given in various sources, e.g., the Abragam book [8]. The response of alkali-metal atomic spins S to magnetic fields can be described by

$$\frac{d\mathbf{S}}{dt} = \gamma \mathbf{S} \times \mathbf{B}, \tag{1}$$

where $\mathbf{S}$ is the electron spin vector, $\mathbf{B}$ is an applied magnetic field, and γ is the gyromagnetic ratio of alkali-metal atoms. By multiplying the above equation by $\mathbf{S}$, we can find that

$$d\mathbf{S}^2 = 0. \tag{2}$$

Hence, the magnitude of $\mathbf{S}$ is the constant of motion, if relaxation is neglected. The time variation of $\mathbf{B}$ can be written by

$$\frac{d\mathbf{B}}{dt} = \mathbf{\Omega} \times \mathbf{B} + \Omega_1 \mathbf{B}, \tag{3}$$

where $\mathbf{\Omega}$ is the vector of rotation of the field and Ω_1 is the constant giving the rate of change of the field without rotation. It can be shown that when the variation of $\mathbf{\Omega}$ is sufficiently slow, precisely when the Fourier component is small at the frequency of order $|\gamma B(t)|$, then in the frame where the spins are aligned along the field $\mathbf{B}$, the change of the spin will be small:

$$|\Delta S_z| \sim \left| \frac{S\Omega}{\gamma B} \right| \ll S. \tag{4}$$

This means that the component of $\mathbf{S}$ along the field $\mathbf{B}$ will remain constant. In other words, if the magnetic field rotates slowly, then the spins will follow the direction of the magnetic field. This can be demonstrated by solving numerically the Bloch equation. This theorem can be reformulated in the reference frame of an atomic magnetometer with one large magnetic field applied along the pump beam direction, B_z, and with a magnetic field oscillating at ω applied along the probe beam direction, $B_x \sin(\omega t)$, as illustrated in Fig. 1.

The adiabatic condition will require that $\omega << \gamma B_z$. Then S_x/S_z will be the same as B_x/B_z; S_y, on the other hand, will

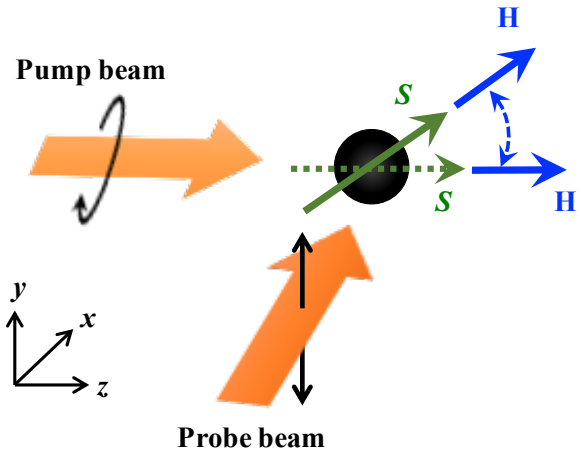

Fig. 1. Configuration of the adiabatic magnetometer: the pump beam is along the z axis; the probe beam along the x axis; and the magnetic field oscillating in the xz plane. The electron spins are following the magnetic field direction.

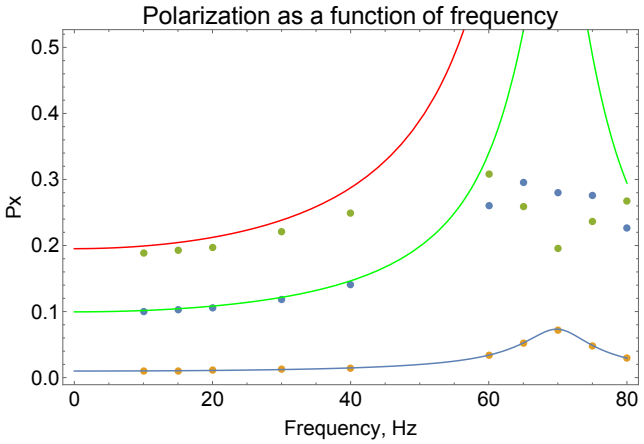

Fig. 2. Comparison of Bloch equation simulations (circular points) with analytical solution (solid curves) obtained in the assumption of small excitation field [Eqs. (5) and (6)]. The excitation fields, B_x are progressively increased from 10^{-6} G (the lowest curve and points) to 10^{-5} G (the middle curve and points) and to 2×10^{-5} G (the upper curve and points). $B_z = 10^{-4}$ G corresponding to the resonance frequency of 70 Hz. The lowest curve is in very close agreement with simulations, while with the increase of the excitation amplitude, the agreement becomes poor, especially near the resonance. The adiabatic following theory works at low frequency even for larger amplitudes

be much smaller than S_x. By solving the Bloch equation and plotting $P_x = 2S_x$ as the function of frequency $\omega/2\pi$ (Fig. 2), it can be seen that this remains true until ω approaches γB_z. If B_x is small, it is possible also to derive an analytical solution that includes the counter-rotating component:

$$S_x^{\rm in} = S_0\gamma B_x\left(\frac{1}{2}\frac{(\omega_0-\omega)}{(\omega-\omega_0)^2+\Gamma^2}+\frac{1}{2}\frac{(\omega_0+\omega)}{(\omega+\omega_0)^2+\Gamma^2}\right), \tag{5}$$

$$S_x^{\rm out} = S_0\gamma B_x\left(\frac{1}{2}\frac{\Gamma}{(\omega-\omega_0)^2+\Gamma^2}-\frac{1}{2}\frac{\Gamma}{(\omega+\omega_0)^2+\Gamma^2}\right), \tag{6}$$

$$S_y^{\rm out} = S_0\gamma B_x\left(\frac{1}{2}\frac{(\omega_0-\omega)}{(\omega-\omega_0)^2+\Gamma^2}-\frac{1}{2}\frac{(\omega_0+\omega)}{(\omega+\omega_0)^2+\Gamma^2}\right), \tag{7}$$

$$S_y^{\rm in} = S_0\gamma B_x\left(\frac{1}{2}\frac{\Gamma}{(\omega-\omega_0)^2+\Gamma^2}+\frac{1}{2}\frac{\Gamma}{(\omega+\omega_0)^2+\Gamma^2}\right). \tag{8}$$

Here $S_0 = S_z$ is the spin polarization owing to optical pumping by the pump beam; $\Gamma = 1/T_2$ is transverse relaxation rate with T_2 being the transverse relaxation time; $\omega_0 = \gamma B_z$ is the Larmor precession frequency; "in" and "out" denote in-phase and out-of-phase components, that are the components oscillating as sine and cosine, respectively. These equations are useful for quantitative analysis of all frequency range.

In the limit of small frequency, so that ω is much smaller than ω_0, the x component of the spin polarization vector is

$$S_x = S_0\gamma B_x\frac{1}{\omega_0} = S_0\frac{B_x}{B_z} \tag{9}$$

as expected. On the other hand, the y component,

$$S_y = S_0\gamma B_x\left(\frac{\Gamma}{\omega_0^2}\right) = S_0\gamma B_x\frac{\Gamma B_x}{(\gamma B_z)^2}, \tag{10}$$

will be much smaller, with the ratio of

$$\frac{S_y}{S_x} = \frac{\Gamma}{\gamma B_z}. \tag{11}$$

The smallness of the y component means adiabatic following, since the rotating field component would include the y component and some phase delay. It is important to note that the rotating wave approximation breaks down and the counter-rotating component (with resonant frequency $-\omega_0$) is really necessary. Otherwise, the amplitude will be only one half of the true value. The y component, unlike the x component, is cancelled by the counter-rotating component.

Figure 2 is given for a relatively low value of B_z, which would result in adiabatic following up to 40 Hz, with nearly constant response. However, the frequency range limitation scales with B_z, and for $B_z = 1$ G, the adiabatic following will be extended to 400 kHz, making the adiabatic magnetometer really broadband.

B. Sensitivity of Adiabatic Magnetometer

The sensitivity analysis of the adiabatic magnetometer is similar to that of the RF atomic magnetometer [6]. To evaluate the relative contributions of the noise, it is convenient to write the fundamental noise equation for the RF magnetometer in the following form:

$$dB = \frac{1}{\gamma\sqrt{nV}}\sqrt{\frac{1}{T_2}+\frac{R_{pr}OD}{8}+\frac{8}{R_{pr}ODT_2^2\eta}}, \tag{12}$$

where n is the atomic spin number density, V is the active volume defined by intersections of the pump and probe beams inside the vapor cell, OD is the optical depth, R_{pr} is the probe pumping rate (it is also the spin destruction rate due to the probe beam), and η is the efficiency of the photo-detector. The adiabatic magnetometer has the first two terms the same,

while the last term needs to be modified. The last term can be found using the equation for the optical rotation ϕ,

$$\phi = \frac{1}{2} l r_e f n P_x D(\nu) \tag{13}$$

where l is the path length, r_e is the classical electron radius, f is the oscillator strength of the transition, 1/3 in case of the D1 line, $P_x = 2S_x$, $D(\nu) = (\nu - \nu_0)/[(\nu - \nu_0)^2 + (\Delta\nu/2)^2]$ is the Lorentzian dispersion profile, assuming that collisional broadening dominates, ν is the laser frequency, ν_0 is the D1 center frequency, and $\Delta\nu$ is optical full width at half maximum (FWHM). For the resonant RF atomic magnetometer operation,

$$P_x = (1/2)\gamma B_1 T_2, \tag{14}$$

while the adiabatic magnetometer has

$$P_x = B_1/B_z. \tag{15}$$

For simplicity we assumed $P_0 = 1$. Thus the adiabatic magnetometer sensitivity is found by substituting T_2 with $2/\gamma B_z$ in the last term,

$$dB = \frac{1}{\gamma\sqrt{nV}} \sqrt{\frac{1}{T_2} + \frac{R_{pr}OD}{8} + \frac{2(\gamma B_z)^2}{R_{pr}OD\eta}}. \tag{16}$$

This equation can be minimized with respect to $R_{pr}OD$, $[R_{pr}OD]_{opt} = \frac{4\gamma B_z}{\sqrt{\eta}}$, giving

$$dB = \frac{1}{\gamma\sqrt{nV}} \sqrt{\frac{1}{T_2} + \frac{\gamma B_z}{\sqrt{\eta}}}. \tag{17}$$

Owing to non-resonant operation, $2/\gamma B_z$ in the adiabatic magnetometer is much shorter than T_2 in the RF atomic magnetometer, so the first term can be neglected and

$$dB = \frac{1}{\gamma\sqrt{nV}} \sqrt{\frac{\gamma B_z}{\sqrt{\eta}}} \tag{18}$$

For $V = 1$ cm^3, $n = 10^{14}$ cm^{-3}, $B_z = 500$ mG, this expression gives 10 fT/Hz$^{1/2}$.

Also, it can be useful to have the photon-shot noise expression for un-optimized $R_{pr}OD$:

$$dB = \frac{B_z}{\sqrt{nV}} \sqrt{\frac{2}{R_{pr}OD\eta}}. \tag{19}$$

One way to estimate the photon-shot noise of the adiabatic magnetometer is by scaling the RF atomic magnetometer noise by $T_2\gamma B_z/2$. For example, a typical RF atomic magnetometer has $T_2 = 10^{-3}$ s and sensitivity of 0.11 fT/Hz$^{1/2}$ [6]; thus for $\gamma B_z = 2\pi \times 700$ Hz (1 mG field), the scaling coefficient is 1.54 resulting in 0.17 fT/Hz$^{1/2}$. If the adiabatic magnetometer is operated in the Earth field, 500 mG, then the sensitivity according to Eq. 19 will be 85 fT/Hz$^{1/2}$, which is somewhat worse than that of the R_{pr}OD-optimized adiabatic magnetometer, 10 fT/Hz$^{1/2}$.

The adiabatic magnetometer is less sensitive to the pump beam spin destruction rates, so the pump power can be increased to compensate for the reduction in the polarization due to the probe beam spin destruction rate, R_{pr}. Therefore in addition to increasing the $R_{pr}OD$ via R_{pr}, it is necessary to increase the pumping rate. This would lead to T_2 shortening, but for large B_z, the effect on the sensitivity will be small. The other parameter is the density. Increase in the density leads to the increase in the spin-destruction R_{SD} and spin-exchange rates R_{SE} due to alkali-alkali collisions. Because $1/T_2 = \sqrt{R_{SD}R_{SE}/5}$, the increase in sensitivity of the RF magnetometer due to the density cancels when the spin-destruction R_{SD} rate dominates by alkali-alkali collisions. In case of the adiabatic magnetometer, the increase in density can lead to proportional gain in sensitivity in some range, because the spin noise that depends on T_2 can be neglected. Considering all factors for optimization, it is possible to have an adiabatic magnetometer with 1 fT/Hz$^{1/2}$ sensitivity with bandwidth of 10 kHz. Another useful advantage is that the adiabatic magnetometer is sensitive to only one field component, mainly B_x (along the probe beam). This can be useful for shields or system that can minimize noise for one component. For many applications it can be assumed that the adiabatic magnetometer is not sensitive to B_y, with the sensitivity suppressed by a factor $\Gamma/\gamma B_z$, which can be large. The adiabatic magnetometer signal also depends on B_z, in the combination B_x/B_z. Assuming that B_x is small, the B_z noise contribution to the signal will be also small.

III. Applications

A. Biomagnetic Sensing

Atomic magnetometers became a popular substitute for cryogenic superconducting quantum interference devices (SQUIDs) for biomagnetic sensing, especially magneto-encephalography (MEG) [10] and magnetocardiography (MCG) [11]. While the SERF magnetometer set the record at low frequency, its high sensitivity comes at the expense of narrow bandwidth and special zero-field requirements, which in its turn requires multi-layer magnetic shielding. The adiabatic magnetometer, which potentially can achieve sub fT sensitivity, does not require field zeroing, and can operate with some field offsets and gradients, provided they are not too large. This is because the sensitivity of the adiabatic magnetometer optimized with $R_{pr}OD$ is reduced as square root of the DC field. The gradients do not affect the operation if they are smaller than the bias field. Thus sensitive measurements can be implemented in a simpler shield systems or even unshielded environment. The high sensitivity relies on the performance of the probe laser close to the photon shot noise limit, as can be implied from the sensitivity theory presented in the previous section. Usually the lasers have $1/f$ technical noise, so modulation of the signal is desirable to shift the operation toward higher frequency, where laser noise approaches the shot-noise limit. The adiabatic magnetometer signal depends on the ratio of B_x to B_z, so modulation of B_z will lead to shifting the B_x spectrum to the sidebands of the modulation frequency. On the other hand, B_x can be modulated to do similar shift of the B_z spectrum. With modulations at two

different frequencies, B_x and B_z can be measured at the same time. The sensitivity limit will be of similar order as that of the adiabatic magnetometer estimated in the previous section.

B. NMR Detection

One case where it is quite difficult to use a resonant magnetometer is nuclear magnetic resonance (NMR) detection, because a bias field is applied for a specific NMR frequency. For example, if 1 mG field is applied, NMR frequency will be 4.26 Hz. As we discussed earlier, 1 mG field reduces sensitivity to 0.17 fT level (obtained from scaling the sensitivity of the RF magnetometer), which is much superior over the sensitivity of coils. On the other hand, for 0.5 G field (2.13 kHz NMR precession), the sensitivity would drop to the level of 10 fT for 1 cm^3 vapor cell, which is still better than the coil sensitivity of a similar size.

For higher NMR frequencies, for example, 42.6 kHz (10 G field), to improve the sensitivity, it is possible to insert the magnetometer inside a long solenoid to compensate the field to some level, perhaps to 0.5 G, which would lead to 10 fT sensitivity and 300 kHz bandwidth. Because the adiabatic magnetometer is not sensitive to gradients and accuracy of the field and stability, it will operate with high sensitivity inside even imperfect solenoid. Previously, we were using a solenoid to create field in the NMR sample, and this lead to gradients and dephasing, not to mention to restrictions imposed on the sample. The drawback of the inserting the adiabatic magnetometer into the solenoid will be the solenoid noise, coming from the current and Johnson noise of wires. Thin wires and low-pass filters can be used to reduce the Johnson noise.

C. Atomic Density Measurements

The adiabatic magnetometer can be useful for measuring alkali-metal density inside a vapor cell. Because the signal is proportional to the density (Eq. 13), quite independently of the width of the magnetic resonance, which can be result of multiple factors such as gradients, spin-destruction rates, pump and probe beam parameters, etc, the signal can be used to monitor relative or absolute density. For absolute density measurements, it is also necessary to know the detuning of the probe laser, approximate pump level, ideally saturating P_z to 1.

We have used the adiabatic magnetometer to measure relative density in our rubidium (Rb) vapor cell made of fused silica that does not work as expected (Fig.3). By plotting the adiabatic magnetometer signal vs. the density expected from the vapor density equation, which depends on the vapor cell temperature, it was possible to conclude that Rb vapor density was much below the expected value. One possible reason is that Rb atoms can react with fused silica cell's walls. As this vapor density test, the adiabatic magnetometer is useful for a quick evaluation of vapor cells.

D. Electromagnetic induction imaging

Electromagnetic induction imaging (EII) with atomic magnetometers became recently popular [12]. EII for example

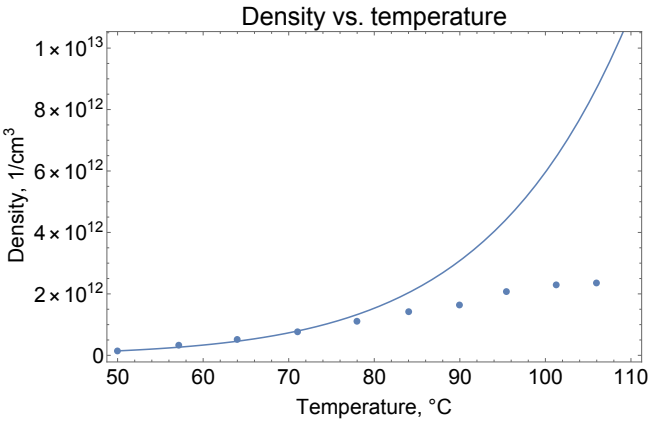

Fig. 3. Comparison of measured density using adiabatic magnetometer signals (circular points) with expected density with the saturation density equation (solid curve) for a Rb vapor cell. This vapor cell for some reason has much lower Rb vapor density than expected, probably due to fused silica material of the cell walls with which it is known that Rb can interact.

can be used to replace X-ray imaging for screening airport baggage. EII has the advantage that no ionizing radiation is emitted. Because of skin depth limitations, frequencies below 1 MHz can be needed where atomic magnetometers can over perform coils. Because also the adiabatic magnetometer can be operated with minimal shielding requirements, it can be suitable for installing in airports and other places. Other applications that rely on conductivity of materials, such as underwater surveillance, biomedical imaging, and brain-injury detection, can also benefit from the adiabatic magnetometer simplified requirements for the operation. Broad-band nature can be benefit for parallel imaging at different frequencies.

IV. Conclusions

While conventional atomic magnetometers are based on resonant operation, with their response enhanced by the magnetic spin resonance, the magnetometers based on the adiabatic following can have valuable properties and advantages as well. We showed that the adiabatic magnetometer is able to reach fT high sensitivity with a very large bandwidth on the order of 10 kHz, in contrast to the resonant atomic magnetometers with a much more limited bandwidth below 1 kHz. The adiabatic magnetometer, owing to its insensitivity to gradients, can also operate in unshielded environment. Some applications of the adiabatic magnetometers, such as biomagnetic field detection, NMR detection, and alkali-metal density measurements, were briefly discussed. For example, it should be possible to detect brain magnetic field in an open environment, but this requires careful optimization of the adiabatic magnetometer: the probe laser noise reduction with modulation, gradiometry. NMR detection at low frequency can be possible with the NMR offset field, but for higher frequencies, the adiabatic magnetometer can be inserted into a solenoid to improve sensitivity.

ACKNOWLEDGMENT

This work was supported by the Los Alamos National Laboratory LDRD Office through Grant No. 20210254ER.

REFERENCES

[1] E. B. Alexandrov and A. K. Vershovskiy, "Mx and Mz magnetometers," Chapter 4 in Optical Magnetometry, Edited by Dmitry Budker and Derek F. Jackson Kimball, Cambridge University Press, 2013.

[2] D. F. Jackson Kimball, S. Pustelny, V. V. Yashchuk, and D. Budker, Chapter 6 in in Optivcal Magnetometry, Edited by Dmitry Budker and Derek F. Jackson Kimball, Cambridge University Press, 2013.

[3] R. E. Slocum and F. N. Reilly, IEEE Trans. Magn. MAG9, 221 (1973).

[4] J. C. Allred, R. N. Lyman, T. W. Kornack, and M. V. Romalis, "High-Sensitivity Atomic Magnetometer Unaffected by Spin-Exchange Relaxation," Phys. Rev. Lett. 89, 130801-1, (2002).

[5] I. Savukov and S. J. Seltzer, "Spin-exchange-relaxation-free (SERF) magnetometer, " Chapter 5, in Optivcal Magnetometry, Edited by Dmitry Budker and Derek F. Jackson Kimball, Cambridge University Press, 2013.

[6] Igor M Savukov, SJ Seltzer, MV Romalis, KL Sauer, "Tunable Atomic Magnetometer for Detection of Radio-Frequency Magnetic Fields, " Phys. Rev. Lett. 95, 063004 (2005).

[7] S. J. Smullin, I. M. Savukov, G. Vasilakis, R. K. Ghosh, and M. V. Romalis, "Low-noise high-density alkali-metal scalar magnetometer,"Phys. Rev. A 80, 033420 (2009).

[8] A. Abragam, "Principles of Magnetic Resonance," International Series of Monographs on Physics, Oxford University Press, 2006.

[9] S.-K. Lee, K. L. Sauer, S. J. Seltzer, O. Alem, and M. V. Romalis, "Subfemtotesla radio-frequency atomic magnetometer for detection of nuclear quadrupole resonance," Appl. Phys. Lett. 89, 214106 (2006).

[10] H. Xia, A. Ben-Amar Baranga, D. Hoffman, and M. V. Romalis, "Magnetoencephalography with an atomic magnetometer,"Appl. Phys. Lett. 89, 211104 (2006).

[11] Young Jin Kim, Igor Savukov, Shaun Newman, "Magnetocardiography with a 16-channel fiber-coupled single-cell Rb optically pumped magnetometer," Appl. Phys. Lett. 114, 143702 (2019).

[12] Luca Marmugi and Ferruccio Renzoni, "Electromagnetic Induction Imaging with Atomic Magnetometers: Progress and Perspectives," Appl. Sci. 10, 6370 (2020); doi:10.3390/app10186370